HISTOGRAMS AND ALL THAT

WOLFHARD JANKE
Institut für Theoretische Physik, Universität Leipzig
Augustusplatz 10/11, D-04109 Leipzig, Germany

Abstract. In this lecture we first discuss "static" single- and multiple-histogram reweighting methods and then move on to "dynamic" updating methodologies related to histogramming. Specifically we will consider the multicanonical approach and tempering methods. The methods are illustrated with applications to systems exhibiting first-order phase transitions and spin glasses.

1. Introduction

Numerical Monte Carlo simulations can be roughly divided into two parts: *i*) data generation and *ii*) data analyses. The two parts are, of course, not completely independent, but interfere and influence each other. A typical example for this mutual influence are "static" histogram reweighting methods (data analysis tools) and "dynamic" update methodologies based on generalized ensembles (data generation algorithms). Both types of algorithms are completely general which makes them so useful and powerful.

In this lecture we will begin with a discussion of single- and multiple histogram techniques in Sects. 2 and 3, respectively. Section 4 is devoted to the multicanonical update procedure. The usefulness of this method is demonstrated by applications to first-order phase transitions and spin glasses. In Sect. 5 related tempering methods are discussed, and in Sect. 6 a brief summary is given.

2. Single-histogram technique

The single-histogram reweighting technique [1] is based on the following very simple observation. If we denote the number of states (spin configurations) that have the same energy E by $\Omega(E)$, the partition function at the simulation point $\beta_0 = 1/k_B T_0$ can always be written as[1]

$$Z(\beta_0) = \sum_{\{s\}} e^{-\beta_0 H(\{s\})} = \sum_E \Omega(E) e^{-\beta_0 E} \propto \sum_E P_{\beta_0}(E) \ , \tag{1}$$

where we have introduced the unnormalized energy histogram (density)

$$P_{\beta_0}(E) \propto \Omega(E) e^{-\beta_0 E} \ . \tag{2}$$

If we would normalize $P_{\beta_0}(E)$ to unit area, the r.h.s. would have to be divided by $\sum_E P_{\beta_0}(E) = Z(\beta_0)$, but the normalization will be unimportant in what follows. Let us assume we have performed a Monte Carlo simulation at inverse temperature β_0 and thus know $P_{\beta_0}(E)$. It is then easy to see that

$$P_\beta(E) \propto \Omega(E) e^{-\beta E} = \Omega(E) e^{-\beta_0 E} e^{-(\beta-\beta_0)E} \propto P_{\beta_0}(E) e^{-(\beta-\beta_0)E} \ , \tag{3}$$

i.e., the histogram at any point β can be derived, in principle, by *reweighting* the simulated histogram at β_0 with the exponential factor $\exp[-(\beta-\beta_0)E]$. Notice that in reweighted expectation values,

$$\langle f(E)\rangle(\beta) = \sum_E f(E) P_\beta(E) / \sum_E P_\beta(E) \ , \tag{4}$$

the normalization of $P_\beta(E)$ indeed cancels. This gives for instance the energy $\langle e\rangle(\beta) = \langle E\rangle(\beta)/V$ and the specific heat $C(\beta) = \beta^2 V[\langle e^2\rangle(\beta) - \langle e\rangle^2(\beta)]$, in principle, as a continuous function of β from a single Monte Carlo simulation at β_0, where $V = L^d$ is the system size.

As an example of this reweighting procedure, using actual simulation data for the two-dimensional (2D) Ising model at $\beta_0 = \beta_c = \ln(1+\sqrt{2})/2 = 0.440\,686\ldots$ on a 16×16 lattice with periodic boundary conditions, the specific heat $C(\beta)$ is shown in Fig. 1(a) and compared with the curve obtained from the exact Kaufman solution [2, 3] for finite $L_x \times L_y$ lattices. This clearly demonstrates that, in practice, the β-range over which reweighting can be trusted is limited. The reason for this limitation are unavoidable statistical errors in the numerical determination of P_{β_0} using a Monte Carlo simulation. In the tails of the histograms the relative statistical errors are largest, and the tails are exactly the regions that contribute most when multiplying $P_{\beta_0}(E)$ with the exponential reweighting factor to obtain $P_\beta(E)$ for β's far off the simulation point β_0. This is illustrated in Fig. 1(b) where the simulated histogram at $\beta_0 = \beta_c$ is shown together with the reweighted histograms at $\beta = 0.375 \approx \beta_0 - 0.065$ and $\beta = 0.475 \approx \beta_0 + 0.035$, respectively. Here the quality of the histograms can be judged by comparing with the curves obtained from Beale's [4] exact expression for $\Omega(E)$.

[1] For simplicity we consider here only models with *discrete* energies. If the energy varies continuously, sums have to be replaced by integrals, etc. Also lattice size dependences are suppressed to keep the notation short.

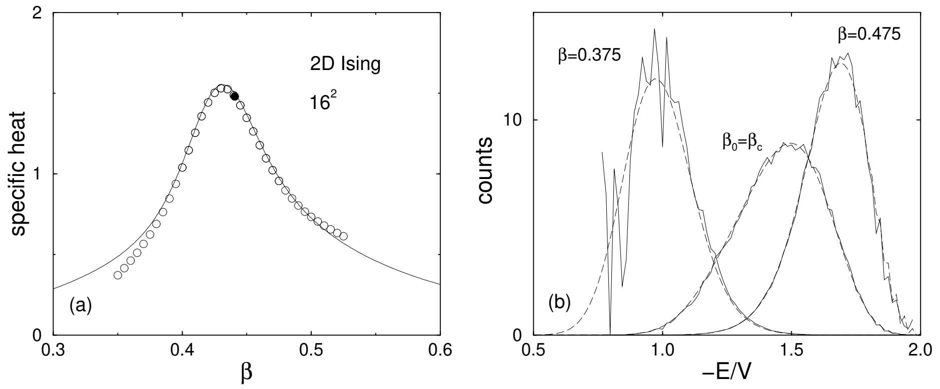

Figure 1. (a) The specific heat of the 2D Ising model on a 16×16 square lattice computed by reweighting from a single Monte Carlo simulation at $\beta_0 = \beta_c$, marked by the filled data symbol. The continuous line shows for comparison the exact solution of Kaufman [2, 3]. (b) The corresponding energy histogram at β_0, and reweighted to $\beta = 0.375$ and $\beta = 0.475$. The dashed lines show for comparison the exact histograms obtained from Beale's [4] expression.

As a rule of thumb, the range over which reweighting should produce accurate results can be estimated by requiring that the peak location of the reweighted histogram should not exceed the energy value at which the input histogram had decreased to about one half or one third of its maximum value. In most applications this range is wide enough to locate from a single simulation, e.g., the specific-heat maximum by employing standard maximization routines to the continuous function $C(\beta)$. This is by far more convenient, accurate and faster than the traditional way of performing many simulations close to the peak of $C(\beta)$ and trying to determine the maximum by spline or least-squares fits.

For an analytical estimate of the reweighting range we now require that the peak of the reweighted histogram is within the width $\langle e\rangle(T_0) \pm \Delta e(T_0)$ of the input histogram (where a Gaussian histogram would have decreased to $\exp(-1/2) \approx 0.61$ of its the maximum value),

$$|\langle e\rangle(T) - \langle e\rangle(T_0)| \leq \Delta e(T_0) \ , \tag{5}$$

where we have made use of the fact that for a not too asymmetric histogram $P_{\beta_0}(E)$ the maximum location approximately coincides with $\langle e\rangle(T_0)$. Recalling that the half width Δe of a histogram is related to the specific heat via $(\Delta e)^2 \equiv \langle (e - \langle e\rangle)^2\rangle = \langle e^2\rangle - \langle e\rangle^2 = C(\beta_0)/\beta_0^2 V$ and using the Taylor expansion $\langle e\rangle(T) = \langle e\rangle(T_0) + C(T_0)(T - T_0) + \ldots$, this can be written as

$C(T_0)|T-T_0| \le T_0\sqrt{C(T_0)/V}$ or

$$\frac{|T-T_0|}{T_0} \le \frac{1}{\sqrt{V}}\frac{1}{C(T_0)} \ . \tag{6}$$

Since $C(T_0)$ is known from the input histogram this is quite a general estimate of the reweighting range. If we only want to know the scaling behaviour with system size $V = L^d$, we can go one step further by considering three generic cases:

i) *Off-critical*, where $C(T_0) \approx$ const., such that

$$\frac{|T-T_0|}{T_0} \propto V^{-1/2} = L^{-d/2} \ . \tag{7}$$

ii) *Critical*, where $C(T_0) \simeq a_1 + a_2 L^{\alpha/\nu}$, with a_1 and a_2 being constants, and α and ν denoting the standard critical exponents of the specific heat and correlation length, respectively. For $\alpha > 0$, the leading scaling behaviour becomes $|T-T_0|/T_0 \propto L^{-d/2}L^{-\alpha/2\nu}$. Assuming hyperscaling ($\alpha = 2 - d\nu$) to be valid, this simplifies to

$$\frac{|T-T_0|}{T_0} \propto L^{-1/\nu} \ , \tag{8}$$

i.e., the typical scaling behaviour of pseudo-transition temperatures in the finite-size scaling regime of a second-order phase transition [5]. For $\alpha < 0$, the leading scaling behaviour is as in the off-critical case.

iii) *First-order transitions*, where $C(T_0) \propto V$. This yields

$$\frac{|T-T_0|}{T_0} \propto V^{-1} = L^{-d} \ , \tag{9}$$

which is again the typical finite-size scaling behaviour of pseudo-transition temperatures close to a first-order phase transition [6].

If we also want to reweight other quantities such as the magnetization $\langle m \rangle$ we have to go one step further. The conceptually simplest way would be to store two-dimensional histograms $P_{\beta_0}(E, M)$ where $M = Vm$ is the total magnetization. We could then proceed in close analogy to the preceding case, and even reweighting to non-zero magnetic field h would be possible, which enters via the Boltzmann factor $\exp(\beta h \sum_i s_i) = \exp(\beta h M)$. However, the storage requirements may be quite high (of the order of V^2), and it is often preferable to proceed in the following way. For any function $g(M)$, e.g., $g(M) = M^k$, we can write

$$\begin{aligned} \langle g(M) \rangle &= \sum_{\{s\}} g(M(\{s\}))e^{-\beta_0 H}/Z(\beta_0) \\ &= \sum_{E,M} \Omega(E,M) g(M) e^{-\beta_0 E}/Z(\beta_0) \\ &= \sum_{E} \frac{\sum_M g(M)\Omega(E,M)}{\sum_M \Omega(E,M)} \sum_M \Omega(E,M) e^{-\beta_0 E}/Z(\beta_0) \qquad (10) \\ &= \sum_E \langle\langle g(M) \rangle\rangle(E) \Omega(E) e^{-\beta_0 E}/Z(\beta_0) \\ &= \sum_E \langle\langle g(M) \rangle\rangle(E) P_{\beta_0}(E) \ , \end{aligned}$$

where $\Omega(E) = \sum_M \Omega(E,M)$, and

$$\langle\langle g(M) \rangle\rangle(E) = \frac{\sum_M g(M)\Omega(E,M)}{\sum_M \Omega(E,M)} \qquad (11)$$

is the *microcanonical* expectation value of $g(M)$ at fixed energy E, sometimes denoted as a "list". Identifying $\langle\langle M \rangle\rangle(E)$ with $f(E)$ in eq. (4), the actual reweighting procedure is precisely as before. Mixed quantities, e.g. $\langle E^k M^l \rangle$, can be treated similarly. One caveat of this method is that one has to decide beforehand which "lists" $\langle\langle g(M) \rangle\rangle(E)$ one wants to store during the simulation, e.g., which powers k in $\langle\langle M^k \rangle\rangle(E)$ are relevant.

An alternative and more flexible method is based on time series. Suppose we have performed a Monte Carlo simulation at β_0 and stored the time series of N measurements $E_1, E_2, \ldots, E_N$ and $M_1, M_2, \ldots, M_N$. Then the most general expectation values at another inverse temperature β can simply be obtained from

$$\langle f(E,M) \rangle = \sum_{i=1}^{N} f(E_i, M_i) e^{-(\beta-\beta_0)E_i} / \sum_{i=1}^{N} e^{-(\beta-\beta_0)E_i} \ , \qquad (12)$$

i.e., in particular all moments $\langle E^k M^l \rangle$ can be computed. Notice that this can also be written as

$$\langle f(E,M) \rangle = \langle f(E,M) e^{-(\beta-\beta_0)E} \rangle_0 / \langle e^{-(\beta-\beta_0)E} \rangle_0 \ , \qquad (13)$$

where the subscript 0 refers to expectation values taken at β_0. Another very important advantage of the last formulation is that it works without any systematic discretization error also for continuously distributed energies and magnetizations.

As nowadays hard-disk space is no real limitation anymore, it is advisable to store time series in any case. This guarantees the greatest flexibility in the data analysis. As far as memory requirements of the actual reweighting code is concerned, however, the method of choice is sometimes not so clear. Using directly histograms and lists, one typically has to store about $(6-8)V$ data, while working directly with the time series one needs $2N$ computer words. The cheaper solution (also in terms of CPU time) thus obviously depends on both, the system size V and the run length N. It is hence sometimes faster to generate from the time series first histograms and the required lists and then proceed with reweighting the latter quantities.

3. Multi-histogram technique

The basic idea of the multi-histogram technique [7] can be summarized as follows:

i) Perform m Monte Carlo simulations at $\beta_1, \beta_2, \ldots, \beta_m$ with N_i, $i = 1, \ldots, m$, measurements,
ii) reweight all runs to a common reference point β_0,
iii) combine at β_0 all information by computing error weighted averages,
iv) reweight the "combined histogram" to any other β.

Here we shall assume that the histograms $P_{\beta_i}(E)$ are "naturally" normalized, $\sum_E P_{\beta_i}(E) = N_i$, such that the statistical errors for each of the histograms $P_{\beta_i}(E)$ are approximately given by $\sqrt{P_{\beta_i}(E)}$. By choosing as reference point $\beta_0 = 0$ and working out the error weighted combined histogram one ends up with

$$\Omega(E) = \frac{\sum_{i=1}^{m} P_{\beta_i}(E)}{\sum_{i=1}^{m} N_i Z(\beta_i)^{-1} e^{-\beta_i E}} \,, \tag{14}$$

where the unknown partition function values $Z(\beta_i)$ are determined self-consistently from

$$Z(\beta_i) = \sum_E \Omega(E) e^{-\beta_i E} = \sum_E e^{-\beta_i E} \frac{\sum_{k=1}^{m} P_{\beta_k}(E)}{\sum_{k=1}^{m} N_k Z(\beta_k)^{-1} e^{-\beta_k E}} \,, \tag{15}$$

up to an unimportant overall constant. In order to work in practice, the histograms at neighbouring β-values must have sufficient overlap, i.e., the spacings of the simulation points must be chosen according to the estimates (7)-(9).

Multiple-histogram reweighting has been widely applied in many different applications. Some problems of this method are that autocorrelations cannot properly be taken into account when computing the error weighted average (which is still correct but no longer optimized), the procedure for computing mixed quantities such as $\langle E^k M^l \rangle$ is difficult to justify (even so it does work as an "ad hoc" prescription quite well), and the statistical error analysis becomes quite cumbersome.

As an alternative one may compute by reweighting from each of the m simulations all quantities of interest as a function of β, including their statistical error bars which now also should take care of autocorrelations [8]. In this way one obtains, at each β-value, m estimates, e.g. $e_1(\beta) \pm \Delta e_1, e_2(\beta) \pm \Delta e_2, \ldots, e_m(\beta) \pm \Delta e_m$, which may be optimally combined according to their error bars to give $e(\beta) \pm \Delta e$ [9]. Notice that in this way the average for each quantity is individually optimized.

4. Multicanonical simulations

By applying multi-histogram reweighting to m canonical simulations at $\beta_1 < \beta_2 < \ldots < \beta_m$ with overlapping histograms, the density of states $\Omega(E)$ can be determined (up to an overall constant) roughly in the range $E(\beta_m) < E < E(\beta_1)$. Once $\Omega(E)$ is known, canonical quantities can be computed by standard reweighting. Reliable results can be expected in the range $\beta_1 < \beta < \beta_m$. Of course, since the individual histogram widths decrease with increasing system size [recall eqs. (7)-(9)], in the large volume limit more and more simulation points are necessary to cover the same energy range with overlapping histograms.

Multicanonical simulations [10, 11] may be interpreted as a method of achieving such a combined statistics over an extended energy range in a *single* simulation run, instead of patching *many* independent canonical simulations in the way described above. This interpretation is stressed by the notation used in the original papers by Berg and Neuhaus [12, 13] and explains the name "*multi*canonical". At the same time, their method may also be viewed as a specific realization of non-Boltzmann sampling which has been known since long to be a legitimate alternative to the more standard Monte Carlo approaches [14]. In this formulation, the multicanonical method appears as a non-standard reweighting approach [15], a view which in most cases simplifies the actual implementation.

The practical significance of non-Boltzmann sampling was first demonstrated a long time ago by Torrie and Valleau [16] with what they called "umbrella sampling". Most of the early applications aimed at a reliable computation of free energies which can be obtained by canonical Boltzmann sampling only indirectly via so-called thermodynamic integration [6]. In the following years attention slowly shifted to the problems of rare-event sampling and quasi-ergodicity [17], but it took many years before the development of the multicanonical scheme [12, 13] turned non-Boltzmann sampling into a widely appreciated practical tool in computer simulation studies. Once the feasibility of such generalized ensemble approach was realized, many related methods were developed.

The multicanonical method implements reweighting at the level of Monte Carlo updating the degrees of freedom. In this sense it may be called a "dynamical" application of histogram reweighting. Conceptually the method can be divided into two main approaches. The first is based on "enhancing the probability of rare event states", which is the typical strategy for dealing with the highly suppressed mixed-phase region of first-order phase transitions [6]. This allows a direct study of properties of the rare event states, for example interface tensions or more generally free energy barriers, which would be very difficult (or practically impossible) with canonical simulations and also with the tempering methods discussed below in Sect. 5. The second approach can be best described by "avoiding rare events" which is closer in spirit to the alternative methods. In this variant one tries to connect the important parts of phase space by "easy paths" which go around the suppressed rare event regions which hence cannot be studied directly.

In both approaches the canonical Boltzmann distribution

$$\mathcal{P}_{\rm can}(\phi) \propto \exp(-\beta H(\phi)) \ , \tag{16}$$

is replaced by an auxiliary distribution

$$\mathcal{P}_{\rm muca}(\phi) \propto \exp(-\beta H(\phi) - f(\{Q_i(\phi)\})) \ , \tag{17}$$

where ϕ denotes the degrees of freedom and $W(\{Q_i\}) \equiv \exp(-f(\{Q_i\}))$ is a reweighting factor. With a suitably chosen $W(\{Q_i\})$, the probability distribution $P_{\rm muca}(\{Q_i\})$ of the macroscopic variables $\{Q_i\}$ can be tuned to take any desired form. The Monte Carlo sampling of $\mathcal{P}_{\rm muca}(\phi)$ proceeds in the usual way by comparing $\beta H(\phi) + f(\{Q_i(\phi)\})$ before and after a proposed update move of ϕ. In most applications local update algorithms have been employed, but for certain classes of models also non-local multigrid methods are applicable [18], which can lead to real-time improvements of the performance by a factor of about ten [19]. A combination with non-local cluster update algorithms, on the other hand, is not straightforward. Only by making direct use of the random-cluster representation as a starting point, a multibondic variant [20] has been proposed. Before discussing the choice of the variables $\{Q_i\}$ and of the reweighting factor $W(\{Q_i\})$, it should be emphasized that, whatever these choices are, canonical expectation values can always be recovered exactly by inverse reweighting,

$$\langle \mathcal{O} \rangle_{\rm can} = \langle \mathcal{O} W^{-1}(\{Q_i\}) \rangle_{\rm muca} / \langle W^{-1}(\{Q_i\}) \rangle_{\rm muca} \ , \tag{18}$$

similar to eq. (13). The performance of the simulation, of course, does depend crucially on the choice of $\{Q_i\}$ and on the form of $W(\{Q_i\})$, since for

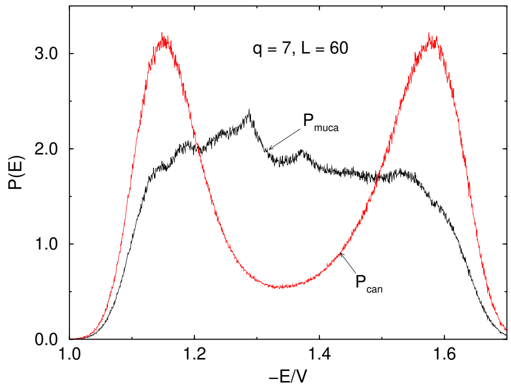

Figure 2. The multicanonical energy density $P_{\rm muca}(E)$ of the 2D 7-state Potts model on a 60×60 lattice together with its canonical energy density $P_{\rm can}(E)$ reweighted to $\beta_{{\rm eqh},L}$ where the two peaks are of equal height.

instance in the special case $W \equiv 1$ one recovers the troublesome canonical ensemble.

The proper identification of the relevant set of Q_i's requires considerable physical intuition and insight into the specific system under study. While for disordered complex systems this is a serious problem, in studies of first-order phase transitions the proper choice is clear. At a temperature-driven transition the energy E is the relevant variable, and at a field-driven transition one should consider the magnetization M or order parameter Q. In the first case, $P_{\rm can}(E)$ exhibits a double-peak structure in the vicinity of the transition point, which becomes more and more pronounced with increasing system size [6]. Here the weight function $f(E)$ in (17) is usually chosen such that the multicanonical energy density $P_{\rm muca}(E) = P_{\rm can}(E)\exp(-f(E))$ is approximately flat between the two peaks of the canonical distribution [10, 11], see Fig. 2. Similarly, in the so-called multimagnetical variant [21, 22] one aims at a flat magnetization distribution, and in the multibondic variant [20], adapted to a combination with cluster algorithms, Q_i is taken as the number of active bonds. At first sight it may appear natural to require that the macroscopic variables Q_i are uniformly sampled. The method is, however, by no means restricted to this choice, and it has in fact been shown that in certain applications non-uniform distributions are more appropriate [23].

4.1. MULTICANONICAL RECURSION

The most important technical point is the procedure for constructing the multicanonical weights W [24, 25, 26, 27, 28, 29, 30]. For a uniform multicanonical distribution the formal solution is $\exp(-f(\{Q_i\})) = P_{\rm can}(\{Q_i\})^{-1}$. Of course, at the beginning the canonical probability distribution on the r.h.s. is not known and one has to proceed by iteration. Starting with the canonical weight, or some initial guess based on results for already simulated smaller systems together with finite-size scaling extrapolations, one performs a short simulation to get an improved estimate of the canonical distribution. When this is inverted one obtains a new estimate of the multicanonical weight factor, which then is used in the next iteration and so on. In this naive version only the simulation data of the last iteration are used in the construction of the improved weight factor.

A more sophisticated recursion, in which the new weight factor is computed from all available data accumulated so far, works as follows. For simplicity we shall consider the case $Q_i = E$ and define $R(E) = W(E + \Delta E)/W(E)$ with $W(E) = \exp(-f(E))$, but the method is completely general [30]:

1. Perform a simulation with $R_n(E)$ to obtain the histogram $H_n(E)$.
2. Compute the statistical weight of the nth run:

$$p(E) = H_n(E)H_n(E + \Delta E)/[H_n(E) + H_n(E + \Delta E)] \ . \tag{19}$$

3. Accumulate statistics:

$$\begin{aligned} p_{n+1}(E) &= p_n(E) + p(E) \ , && (20) \\ \kappa(E) &= p(E)/p_{n+1}(E) \ . && (21) \end{aligned}$$

4. Update weight ratios:

$$R_{n+1}(E) = R_n(E) \, [H_n(E)/H_n(E + \Delta E)]^{\kappa(E)} \ . \tag{22}$$

Goto 1.

The recursion is initialized with $p_0(E) = 0$. Due to the accumulated statistics, this procedure is rather insensitive to the length of the nth run in the first step.

Another, possibly more efficient method, works directly with estimators $\Omega(E)$ of the density of states [31, 32]. By flipping spins randomly, the transition probability from energy level E_1 to E_2 is

$$p(E_1 \to E_2) = \min\left[\frac{\Omega(E_1)}{\Omega(E_2)}, 1\right] \ . \tag{23}$$

Each time an energy level is visited, the estimator is multiplicatively updated,

$$\Omega(E) \to f \, \Omega(E) \ , \tag{24}$$

where initially $\Omega(E) = 1$ and $f = f_0 = e^1$. Once the accumulated energy histogram is sufficiently flat, the factor f is refined,

$$f_{n+1} = \sqrt{f_n} \ , \qquad n = 0, 1, \dots \ , \tag{25}$$

and the energy histogram reset to zero until some small value such as $f = e^{10^{-8}} \approx 1.00000001$ is reached.

For the 2D Ising model this procedure converges very rapidly towards the exactly known density of states, and also for other applications a fast convergence has been reported. Since the procedure is known to violate detailed balance, however, same care is necessary of setting up a proper protocol of the recursion. Most authors who employ the obtained density of states directly to extract canonical expectation values by standard reweighting argue that, once f is close enough to unity, systematic deviations become negligible. While this claim can be verified empirically for the 2D Ising model (where exact results are available for judgement), it is difficult to access in the general case. A safe way would be to consider the recursion (23)-(25) as an alternative method to determine the multicanonical weights, and then to perform a usual multicanonical simulation based on them. As emphasized earlier, any deviations of multicanonical weights from their optimal shape do not show up in the final canonical expectation values; they rather only influence the dynamics of the multicanonical simulations.

To summarize, multicanonical simulations consist of the following steps:

1. Recursive construction of the weights W.
2. A thermalization run with fixed weights.
3. A production run with fixed weights, collecting measurements.
4. Inverse reweighting (18) to extract the desired canonical quantities.

4.2. APPLICATIONS

The multicanonical method is very general and can easily be adapted to a given problem. Consequently the applications span basically the whole spectrum of computational biological, chemical, condensed matter and high energy physics. Instead of giving a list of key words, here we shall discuss only two prototype applications which illustrate the general procedure.

4.2.1. *First-Order Phase Transitions*

The first applications of multicanonical simulations concentrated on investigations of first-order phase transitions [6]. Only later they were also applied to complex systems such as spin glasses discussed below or proteins where the folding mechanism is in the focus of interest [33].

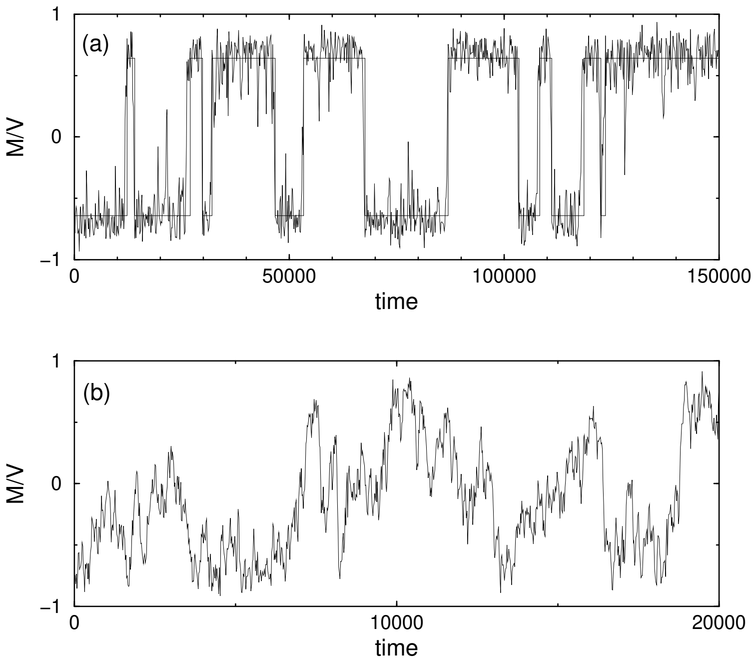

Figure 3. Time evolution of magnetization measurements in (a) canonical and (b) multicanonical simulations of the 2D ϕ^4 lattice model [19].

Phase coexistence at a first-order phase transition is directly related to the double peaked energy or magnetization density. The peaks are governed by the pure phases and the dip in between is associated with the two-phase region containing interfaces. Compared with the peaks, the probability of two-phase configurations is exponentially suppressed by the additional Boltzmann factor $\exp(-2\beta\sigma L^{d-1})$, where σ is the interface tension [6]. In a canonical simulation, the time to pass this interface region is inversely proportional to its likelihood. This leads to the characteristic flip-flop behaviour shown in Fig. 3(a), where the average time spent in each phase between the jumps is a measure for the autocorrelation time. With increasing system size this implies exponentially growing autocorrelation times, $\tau \simeq \exp(2\beta\sigma L^{d-1})$, a behaviour which is often referred to as "supercritical slowing down".

As is illustrated in Fig. 2 for the energy and in Fig. 4 for the magnetization, in a typical application one tries to generate multicanonical weights that render the resulting multicanonical distribution $P_{\rm muca}$ flat between the two peaks of the canonical distribution $P_{\rm can}$. This amounts to enhancing the low probabilities of the "rare-events" in the two-phase region. The left and right tails are usually not of direct physical interest and are left unmod-

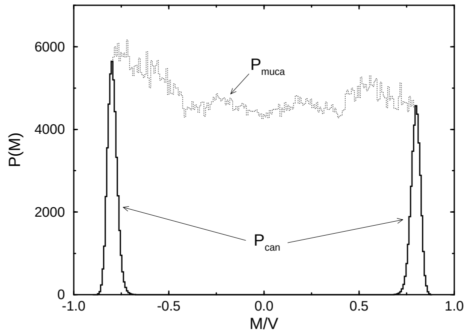

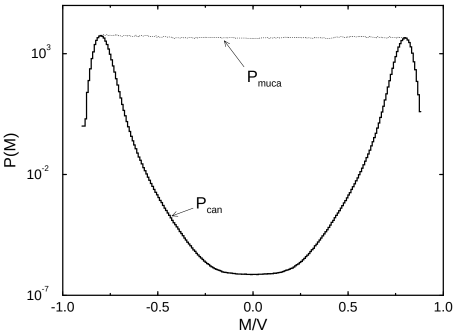

Figure 4. Canonical and multicanonical magnetization densities obtained in multimagnetical simulations of the 2D ϕ^4 lattice model on linear (left) and logarithmic (right) scales [19]. Notice that in this example ($\hat{\sigma} \equiv \beta\sigma = 0.16577(73)$, $L = 64$) the two-phase region is suppressed by about ten orders of magnitude.

ified in order to save computing time. The distance between the two peaks approximately scales with the volume V of the system. If $P_{\rm muca}$ was completely flat between the two canonical peaks and the Monte Carlo update moves would perform an ideal random walk, one would expect that after V^2 local updates the system has travelled on average a distance V in energy or magnetization. Since one lattice sweep consists of V local updates, the autocorrelation time should scale in this idealized picture as $\tau \propto V$. An example for a multicanonical time evolution is shown in Fig. 3(b).

Numerical tests for various models with a first-order phase transition have shown that in practice the data are at best consistent with a behaviour $\tau \propto V^\alpha$, with $\alpha \geq 1$. While for the temperature-driven transitions of 2D Potts models the multibondic variant seems to saturate the bound [20], employing local update algorithms, typical fit results are $\alpha \approx 1.1 - 1.3$, and due to the limited accuracy of the data even a weak exponential growth cannot really be excluded. In fact, at least for the field-driven first-order transition of the 2D Ising model, it is known [34, 35] that even for a perfectly flat multicanonical distribution a "hidden" free energy nucleation barrier leads to an exponential growth of τ, which is, however, much weaker than in the corresponding canonical simulation.

In any case, due to significantly reduced autocorrelation times, multicanonical simulations give much more accurate results in a given computer time [8]. The improved accuracy allowed, for instance, careful tests of finite-size scaling theories for first-order phase transitions [36, 37, 6], studies of the coexistence curve in Lennard-Jones fluids [38], and precise estimations of interface tensions using the relation $\hat{\sigma}(L) \equiv \beta\sigma(L) = \ln(P_{\rm can}^{\rm max}/P_{\rm can}^{\rm min})/(2L^{d-1})$ in combination with finite-size scaling extrapolations [6].

4.2.2. *3D Ising Spin Glass*
As a non-trivial example for applications of multicanonical simulations we shall now consider the Edwards-Anderson [39] Ising (EAI) spin-glass model whose energy is defined as

$$E = -\sum_{\langle ik \rangle} J_{ik}\, s_i s_k \ , \tag{26}$$

where the lattice sum runs over all nearest-neighbour pairs of a d-dimensional (hyper-) cubic lattice of size $V = L^d$ with periodic boundary conditions and the fluctuating spins s_i can take the values ± 1. The coupling constants $J_{ik} = \pm 1$ are quenched, *random* variables taking positive and negative signs, thereby leading to *competing interactions*. This models the two basic ingredients necessary for spin-glass behaviour, namely randomness and competing interactions [40, 41, 42, 43, 44]. As a consequence of the randomly competing interactions no single spin configuration is uniquely favoured by all of the interactions, giving rise to so-called "frustration" and a rugged free-energy landscape with probable regions (free energy valleys) separated by rare-event states (free energy barriers), as sketched in Fig. 5.

The analogue of the magnetization for ferromagnets is the Parisi order parameter [45] defined as

$$q = \frac{1}{V} \sum_{i=1}^{V} s_i^{(1)}\, s_i^{(2)} \ , \tag{27}$$

where the spin superscripts label two independent (real) replicas for the same realization of randomly chosen exchange coupling constants $\mathcal{J} = \{J_{ik}\}$. For given $\mathcal{J}$ the probability density of q is denoted by $P_{\mathcal{J}}(q)$ and thermodynamic expectation values by $\langle \ldots \rangle_{\mathcal{J}}$. To get a better approximation of the infinite system, one usually performs averages over many hundreds or even thousands of (quenched) disorder realizations denoted by

$$P(q) = [P_{\mathcal{J}}(q)]_{\rm av} = \frac{1}{\#\mathcal{J}} \sum_{\mathcal{J}} P_{\mathcal{J}}(q) \ , \qquad [\langle \ldots \rangle_{\mathcal{J}}]_{\rm av} = \frac{1}{\#\mathcal{J}} \sum_{\mathcal{J}} \langle \ldots \rangle_{\mathcal{J}} \ , \tag{28}$$

where $\#\mathcal{J}$ $(\to \infty)$ is the number of realizations considered. Below the freezing temperature, in the infinite-volume limit $V \to \infty$, a non-vanishing part of $P(q)$ between its two delta-function peaks at $\pm q_{\rm max}$ characterizes the mean-field picture [45] of spin glasses, whereas in ferromagnets as well as in the droplet picture [46] of spin glasses $P(q)$ exhibits only the two delta-function peaks. Most studies so far considered mainly the averaged quantities.

For a better understanding of the free-energy barriers sketched in Fig. 5, the probability densities for *individual* realizations $\mathcal{J}$ play the central role.

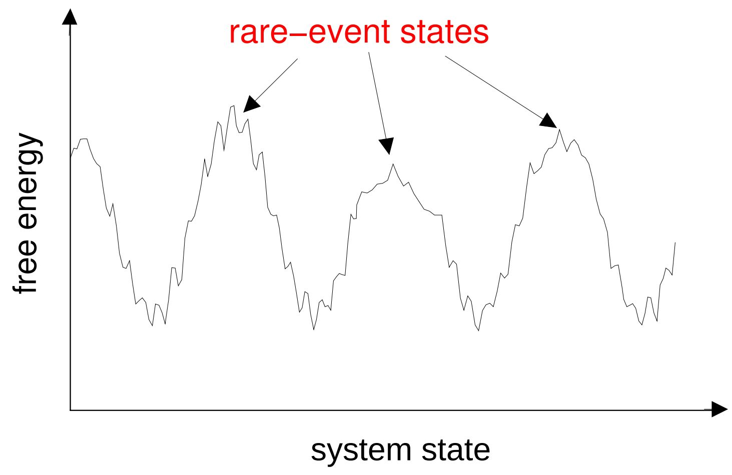

Figure 5. Typical sketch of the rugged free-energy landscape of spin glasses with many valleys separated by rare-event barriers.

It is, of course, impossible to get complete control over the full state space, and to give a well-defined meaning to "system state" (the x-axis in Fig. 5), one has to concentrate on one or a few characteristic parameters. By choosing the overlap q, this leads to multi-overlap simulations [47] with a total weight

$$\mathcal{P}_{\rm muq}(\{s\}) \propto \exp\left[\beta \sum_{\langle ik \rangle} J_{ik}\left(s_i^{(1)}s_k^{(1)} + s_i^{(2)}s_k^{(2)}\right) + S_{\mathcal{J}}(q)\right] \,, \qquad (29)$$

where the two replicas are coupled by the multicanonical weight $W_{\mathcal{J}}(q) = \exp(S_{\mathcal{J}}(q))$. Ideally the weight should satisfy the condition

$$P_{\mathcal{J}}^{\rm muq}(q) = P_{\mathcal{J}}^{\rm can}(q) W_{\mathcal{J}}(q) = {\rm const.}\ , \qquad (30)$$

such that the multi-overlap probability density $P_{\mathcal{J}}^{\rm muq}(q)$ is completely flat over the entire accessible range $-1 \leq q \leq 1$, as sketched in Fig. 6. Since for spin glasses the shapes of $P_{\mathcal{J}}^{\rm can}(q)$ may be quite complicated and strongly vary from realization to realization, it is important to use for the weight determination an automated recursion procedure as described above.

To judge the performance of the algorithm for the three-dimensional (3D) EAI spin-glass model, the autocorrelation times $\tau_{\mathcal{J}}^{\rm muq}$ were fitted to the power-law ansatz $[\tau_{\mathcal{J}}^{\rm muq}]_{\rm av} = c V^{\alpha}$, yielding $\alpha = 2.32(7)$ in the spin-glass phase [48]. This clearly deviates from the theoretical optimum $\alpha = 1$ one would expect for a random-walk behaviour between $q = -1$ and $+1$.

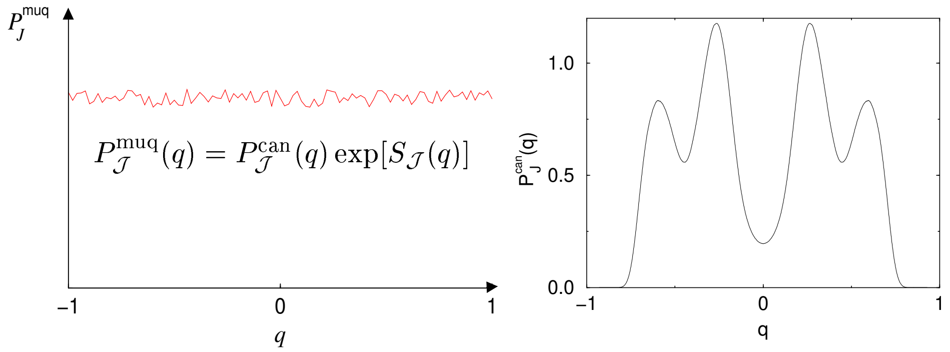

Figure 6. Illustration of the relation between ideally flat multi-overlap densities $P_{\mathcal{J}}^{\mathrm{muq}}(q)$ (left) and canonical densities $P_{\mathcal{J}}^{\mathrm{can}}(q)$ (right) with complicated shapes.

Even an exponential behaviour could hardly be excluded. In multicanonical simulations with flat energy histograms a similarly large exponent of $\alpha = 2.8(1)$ has been observed [49], suggesting that the projection of the multi-dimensional state space onto the q- or E-direction hides important features of the free-energy landscape of the model. An example for this problem has recently been discussed [34] in the much simpler case of field-driven first-order phase transitions in the 2D ferrromagnetic Ising model where the effect of a "hidden" nucleation barrier can be analyzed analytically [35]. Numerical simulations [34] nicely confirmed the theoretically predicted behaviour.

Large-scale multi-overlap simulations of the 3D EAI model led to a variety of new insights, for instance about the self-averaging properties of free energy barriers [48]. The improvements become particularly pronounced in the tails of the distributions, as is demonstrated in Fig. 7. The scaling plot of $P'(q) = \sigma P(q)$ versus $q' = q/\sigma$, where $\sigma \propto L^{-\beta/\nu}$ with $\beta/\nu = 0.230(4)$ $(T = 1)$ and $\beta/\nu = 0.312(4)$ $(T = 1.14)$, respectively, yields at the freezing temperature $T = 1.14$ reliable results over more than 150 orders of magnitude. This allowed us to verify a conjectured relation between the overlap probability density and extreme-order statistics over about 80 orders of magnitude [50]. A similar study for the 3D Ising model, on the other hand, revealed a completely different behaviour [51].

5. Tempering methods

Loosely speaking, tempering methods may be characterized as "dynamical multi-histogramming". Similarly to the static reweighting approach, in "simulated" as well as in "parallel" tempering one considers m simulation points $\beta_1 < \beta_2 < \ldots < \beta_m$ which here, however, are combined already

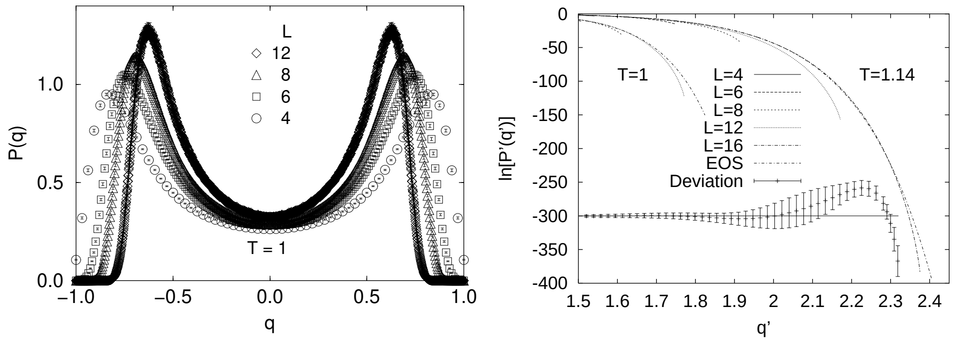

Figure 7. Left: Overlap probability densities for the 3D EAI model in the spin-glass phase. Right: Rescaled densities in comparison with a prediction of extreme-order statistics (EOS) [50].

during the simulation in a specific, dynamical way.

5.1. SIMULATED TEMPERING

In simulated tempering simulations [52, 53] one starts from a joint partition function (expanded ensemble)

$$Z_{\rm ST} = \sum_{i=1}^{m} e^{g_i} \sum_{\{s\}} e^{-\beta_i H(\{s\})} \ , \tag{31}$$

where $g_i = \beta_i f(\beta_i)$ and the inverse temperature β is treated as an additional dynamical degree of freedom that can take the values $\beta_1, \dots, \beta_m$. Employing a Metropolis algorithm, a proposed move from $\beta = \beta_i$ to β_j takes place with probability $\min\left[1, \exp[-(\beta_j - \beta_i)H(\{s\})] + g_j - g_i\right]$. Similar to multi-histogram reweighting (and also to multicanonical simulations), the free-energy parameters g_i are a priori unknown and have to be adjusted iteratively. To assure a reasonable acceptance rate for the β-update moves (usually between neighbouring β_i-values), the histograms at β_i and β_{i+1}, $i = 1, \dots, m-1$, must overlap. An estimate for a suitable spacing $\delta\beta = \beta_{i+1} - \beta_i$ of the simulation points β_i is hence immediately given by the results (7)-(9) for the reweighting range,

$$\delta\beta \propto \begin{cases} L^{-d/2} & \text{off-critical} \ , \\ L^{-1/\nu} & \text{critical} \ , \\ L^{-d} & \text{first-order} \ . \end{cases} \tag{32}$$

Overall the simulated tempering method shows some similarities to the “avoiding rare events” variant of multicanonical simulations.

5.2. PARALLEL TEMPERING

In parallel tempering (exchange Monte Carlo, multiple Markov chain Monte Carlo) simulations [54, 55] the starting point is the product of partition functions (extended ensemble),

$$Z_{\mathrm{PT}} = \prod_{i=1}^{m} Z(\beta_i) = \prod_{i=1}^{m} \sum_{\{s\}_i} e^{-\beta_i H(\{s\}_i)} \ , \tag{33}$$

and all m systems at different simulation points $\beta_1 < \beta_2 < \ldots < \beta_m$ are simulated in parallel, using any legitimate update algorithm (Metropolis, cluster,...). After a certain number of sweeps, exchanges of the current configurations $\{s\}_i$ and $\{s\}_j$ are attempted (equivalently, the β_i may be exchanged, as is done in most implementations). According to a Metropolis criterion the proposed exchange will be accepted with probability $W = \min(1, e^{\Delta})$, where $\Delta = (\beta_j - \beta_i)[E(\{s\}_j) - E(\{s\}_i)]$. To assure a reasonable acceptance rate, usually only "nearest-neighbour" exchanges ($j = i \pm 1$) are attempted and the β_i should again be spaced with the $\delta\beta$ given in (32). In most applications, the smallest inverse temperature β_1 is chosen in the high-temperature phase where the autocorrelation time is expected to be very short and the system rapidly decorrelates. Conceptually this approach follows again the "avoiding rare events" strategy.

Notice that in parallel tempering no free-energy parameters must be adjusted. The method is thus very flexible and moreover can be almost trivially parallelized.

6. Summary

Histogram reweighting techniques have proven to be a very useful tool in Monte Carlo data analyses. Their formulation is very general and hence they are applicable to a wide range of problems. Multicanonical and tempering methods may be viewed as dynamical versions of the multi-histogram method, in which many canonical simulations are combined in a single simulation run. In simulations of first-order phase transitions and complex systems such as spin glasses they have led to enormous improvements. Still, in particular in the latter systems some features of the methods are not yet well understood, which leaves room for further improvements in the future.

Acknowledgments

This work was in part supported by the EC IHP network "EUROGRID: *Discrete Random Geometries: From Solid State Physics to Quantum Gravity* under contract No. HPRN-CT-1999-000161 and the German-Israel-Foundation under contract No. I-653-181.14/1999.

References

1. A.M. Ferrenberg and R.H. Swendsen, Phys. Rev. Lett. **61** (1988) 2635; *ibid.* **63** (1989) 1658 (*Erratum*).
2. B. Kaufman, Phys. Rev. **76** (1949) 1232.
3. A.E. Ferdinand and M.E. Fisher, Phys. Rev. **185** (1969) 832.
4. P.D. Beale, Phys. Rev. Lett. **76** (1996) 78.
5. N. Wilding, *Second-Order Phase Transitions*, this volume.
6. W. Janke, *First-Order Phase Transitions*, this volume.
7. A.M. Ferrenberg and R.H. Swendsen, Phys. Rev. Lett. **63** (1989) 1195.
8. W. Janke, *Statistical Analysis of Simulations: Data Correlations and Error Estimation*, in: Proceedings of the Euro Winter School *Quantum Simulations of Complex Many-Body Systems: From Theory to Algorithms*, edited by J. Grotendorst, D. Marx, and A. Muramatsu, John von Neumann Institute for Computing, Jülich, NIC Series, Vol. **10** (2002), pp. 423–445 [`http://www.fz-juelich.de/nic-series/volume10/janke2.pdf`].
9. C. Holm and W. Janke, Phys. Rev. **B48** (1993) 936.
10. B.A. Berg, *Introduction to Multicanonical Monte Carlo Simulations*, Fields Inst. Comm. **26** (2000) 1 [cond-mat/9909236]; *Generalized Ensemble Simulations for Complex Systems*, Comp. Phys. Comm. **104** (2002) 52.
11. W. Janke, *Multicanonical Monte Carlo Simulations*, Physica **A254** (1998) 164.
12. B.A. Berg and T. Neuhaus, Phys. Lett. **B267** (1991) 249.
13. B.A. Berg and T. Neuhaus, Phys. Rev. Lett. **68** (1992) 9.
14. K. Binder, in: *Phase Transitions and Critical Phenomena*, Vol. 5b, eds. C. Domb and M.S. Green (Academic Press, New York, 1976), p. 1.
15. W. Janke, Int. J. Mod. Phys. **C3** (1992) 1137.
16. G.M. Torrie and J.P. Valleau, Chem. Phys. Lett. **28** (1974) 578; J. Comp. Phys. **23** (1977) 187; J. Chem. Phys. **66** (1977) 1402; I.S. Graham and J.P. Valleau, J. Phys. Chem. **94** (1990) 7894; J.P. Valleau, J. Comp. Phys. **96** (1991) 193.
17. D. Chandler, *Introduction to Modern Statistical Mechanics* (Oxford University Press, Oxford, 1987), pp. 168–175.
18. W. Janke and T. Sauer, Phys. Rev. **E49** (1994) 3475.
19. W. Janke and T. Sauer, J. Stat. Phys. **78** (1995) 759.
20. W. Janke and S. Kappler, Phys. Rev. Lett. **74** (1995) 212; M.S. Carroll, W. Janke, and S. Kappler, J. Stat. Phys. **90** (1998) 1277.
21. B.A. Berg, U. Hansmann, and T. Neuhaus, Phys. Rev. **B47** (1993) 497.
22. B.A. Berg, U. Hansmann, and T. Neuhaus, Z. Phys. **B90** (1993) 229.
23. B. Hesselbo and R. Stinchcombe, Phys. Rev. Lett. **74** (1995) 2151.
24. B.A. Berg and T. Celik, Phys. Rev. Lett. **69** (1992) 2292.
25. J. Lee, Phys. Rev. Lett. **71** (1993) 211; *ibid.* **71** (1993) 2353 (*Erratum*).
26. B.A. Berg, U. Hansmann, and Y. Okamoto, J. Phys. Chem. **99** (1995) 2236.
27. B.A. Berg, J. Stat. Phys. **82** (1996) 323.
28. G.R. Smith and A.D. Bruce, J. Phys. **A28** (1995) 6623; Phys. Rev. **E53** (1996) 6530.
29. M.J. Thill, preprints cond-mat/9703234 and cond-mat/9703233.
30. B.A. Berg and W. Janke, unpublished notes.
31. F. Wang and D.P. Landau, Phys. Rev. Lett. **86** (2001) 2050; Phys. Rev. **E64** (2001) 056101.
32. D.P. Landau, this volume.
33. U.H. Hansmann and Y. Okamoto, J. Comp. Chem. **14** (1993) 1333; M.-H. Hao and H.A. Scheraga, J. Phys. Chem. **98** (1994) 4940; U.H. Hansmann and Y. Okamoto, Ann. Rev. Comp. Phys. **6** (1999) 129; A. Mitsutake, Y. Sugita, and Y. Okamoto, Biopolymers (Peptide Science) **60** (2001) 96.
34. T. Neuhaus and J.S. Hager, preprint cond-mat/0201324.
35. K. Leung and R.K.P. Zia, J. Phys. **A23** (1990) 4593.

36. C. Borgs and S. Kappler, Phys. Lett. **A171** (1992) 37.
37. A. Billoire, T. Neuhaus, and B. Berg, Nucl. Phys. **B396** (1993) 779.
38. N. Wilding, Phys. Rev. **E52** (1995) 602; A.D. Bruce and N. Wilding, preprint cond-mat/0206111, to appear in Adv. Chem. Phys.
39. S.F. Edwards and P.W. Anderson, J. Phys. **F5** (1975) 965.
40. K. Binder and A.P. Young, *Spin Glasses: Experimental Facts, Theoretical Concepts and Open Questions*, Rev. Mod. Phys. **56** (1986) 801.
41. M. Mézard, G. Parisi, and M.A. Virasoro, *Spin Glass Theory and Beyond* (World Scientific, Singapore, 1987).
42. K.H. Fischer and J.A. Hertz, *Spin Glasses* (University Press, Cambridge, 1991).
43. A.P. Young (editor), *Spin Glasses and Random Fields* (World Scientific, Singapore, 1997).
44. W. Janke, B.A. Berg, and A. Billoire, *Multi-Overlap Simulations of Spin Glasses*, in: *NIC Symposium 2001*, edited by H. Rollnik and D. Wolf, John von Neumann Institute for Computing, Jülich, NIC Series, Vol. **9** (2002), pp. 301–314 [`http://www.fz-juelich.de/nic-series/volume9/janke.pdf`].
45. G. Parisi, Phys. Rev. Lett. **43** (1979) 1754.
46. D.S. Fisher and D.A. Huse, Phys. Rev. **B38** (1988) 386.
47. B.A. Berg and W. Janke, Phys. Rev. Lett. **80** (1998) 4771.
48. B.A. Berg, A. Billoire, and W. Janke, Phys. Rev. **B61** (2000) 12143.
49. B.A. Berg, U.E. Hansmann, and T. Celik, Phys. Rev. **B50** (1994) 16444.
50. B.A. Berg, A. Billoire, and W. Janke, Phys. Rev. **E65** (2002) 045102(R).
51. B.A. Berg, A. Billoire, and W. Janke, Phys. Rev. **E66** (2002) 046122.
52. E. Marinari and G. Parisi, Europhys. Lett. **19** (1992) 451.
53. A.P. Lyubartsev, A.A. Martsinovski, S.V. Shevkunov, and P.N. Vorontsov-Velyaminov, J. Chem. Phys. **96** (1992) 1776.
54. C.J. Geyer, in *Computing Science and Statistics*, Proceedings of the 23rd Symposium on the Interface, E.M. Keramidas (editor) (Interface Foundation, Fairfax, Virginia, 1991); pp. 156–163; C.J. Geyer and E.A. Thompson, J. Am. Stat. Assoc. **90** (1995) 909.
55. K. Hukushima and K. Nemoto, J. Phys. Soc. Japan **65** (1996) 1604.